DOI: 10.61782/fa.2023.0953

forum acusticum 2023

PHASE ERROR SENSITIVITY TO THE INVERSION STRENGTH AND DEPTH OF THE BOUNDARY LAYER IN A CONVENTIONALLY NEUTRAL REGIME

Pierangelo Libianchi[1*] **Mark Kelly**[2] **Elena Shabalina**[3]
Finn Agerkvist[1] **Jonas Brunskog**[1]
[1] Acoustic Technology Group, Department of Electrical and Photonics Engineering, Technical University of Denmark, Building 352, Ørsted Plads, DK-2800 Kongens Lyngby, Denmark
[2] Department of Wind Energy, Risø Lab/Campus, Technical University of Denmark, Frederiksborgvej 399, DK-4000 Roskilde, Denmark
[3] Independent researcher

ABSTRACT

In outdoor sound propagation, the variation of wind speed with height plays an important role and a logarithmic profile is often assumed. This is an accurate description in a neutral boundary layer according to MOST. However, the neutral boundary layer can be either truly neutral or conventionally neutral depending on the stability condition at the top of the ABL. While the logarithmic profile is suitable in a truly neutral regime, the conventionally neutral is more commonly found. This regime is characterized by a stable stratification aloft that result in super geostrophic wind speed close to the top of the ABL and higher speed and steeper gradient close to the ground than predicted by the logarithmic profile. This work uses numerical simulations based on the Crank-Nicholson parabolic equation to derive the sensitivity of the phase to the ABL depth and inversion strength as a function of the distance from the source. The results show that a stronger inversion increases the phase differences that can be as large as 60° already at 1 km from the source. Stronger inversions and a deeper ABL produce more complex interference on the ground, showing only after approximately 2 km, that affect both phase and magnitude.

Keywords: *CNBL, outdoor sound propagation, inversion strength, ABL depth, logarithmic profile, phase error*

**Corresponding author*: *pielbia@dtu.dk.*

1. INTRODUCTION

In the atmospheric boundary layer (ABL), the speed of sound generally depends on height. The gradient of the speed of sound defines wave phenomena in the ABL, such as refraction. Atmospheric refraction can cause sound waves from a ground source to bend back to the ground at different rates and create interference patterns with the waves travelling different paths. These effects are important for correct predictions of the sound field close to the ground.

The sound speed profile depends on the wind speed and temperature profiles in the ABL. Depending on the buoyancy at surface level, the ABL can be classified as stable, unstable and neutral. Neutral and quasi-neutral (very small buoyancy) are the most often encountered conditions [1].

In many instances the profiles are assumed to be logarithmic, based on simple similarity theory and surface-layer assumptions [2–4]. In some cases the profiles are just classified by the effect they have on sound propagation, namely upward- or downward-refracting profiles [5, 6]. According to Monin-Obukhov Similarity Theory (MOST), the logarithmic profile is suitable for neutral

regimes [7]. However, Zilitinkevich and Esau [8] distinguishes between a truly and conventionally neutral ABL when considering also the stability conditions at the top of the ABL. In truly neutral conditions, well described by a logarithmic profile, the ABL is neutral both at the top and bottom. In a conventionally neutral boundary layer (CNBL), the ABL presents a stable stratification at the top, in the so called entrainment layer, that results in wind speeds larger than predicted by the logarithmic profile. Furthermore, it produces super-geostrophic wind speed close to the top of the ABL adding a characteristic "nose" to the profile that is commonly known as low-level jet (LLJ, see Figure 1). This latter condition is also the most common of the two [8]. In this paper, we focus on the wind speed in the CNBL since the effect of the stable stratification on the temperature profile is small compared to the adiabatic lapse rate. There are many formulation for the wind profile in a CNBL [9–12]. Liu and Stevens [13] provide a good description that allows to represent a range of inversion strengths and ABL heights.

An accurate description of the phase is crucial when simulating the noise emissions produced from multiple sources and for sound field control applications [14]. However, we have found no such information in the available literature. We investigated the influence that different sections of the wind profile have on the sound field at the ground for one specific ABL depth and inversion strength in a previous work [15]. In this work, we extend that study to investigate how different ABL depths and inversion strengths affect the simulated sound fields.

In this paper, we study the sensitivity of the phase error to the height of the ABL and strength of the inversion at different distances from the source.

We use numerical simulations based on the Crank Nicholson parabolic equation to simulate the sound fields produced by a simple logarithmic profile first, and then by the same profile plus a correction term suitable to a CNBL which we describe in Section 2. We then study the error introduced by neglecting this correction term by comparing the two sound fields using the Modal Assurance Criterion (MAC) and the absolute phase and magnitude errors.

2. THEORY AND METHODS

2.1 Wind profile

To model the wind profile in the CNBL, we use in this work the formulation described in Liu and Stevens [13]. In this section we briefly introduce such formulation, focusing only on the stream-wise component of the wind that is assumed to be parallel to the propagation direction of the sound waves. In this work, we are interested in the effect that the ABL depth h and the inversion strength, described by the Brunt–Väisälä frequency N, have on the prediction of the sound field close to the ground. Here, we use the common assumption that the ABL depth h is related to the height z_t, where the total shear stress reaches 5% of the surface value, through:

$$h = (1 - 0.05^{2/3}) z_t. \tag{1}$$

These two variables are included in the formulation from [13] through the inverse dimensionless boundary height $b = u_*/(fh)$ and the Zilitinkevich number $Zi = N/f$, where f is the Coriolis parameter. The friction velocity u_* in the CNBL is proportional to $h(fN)^{1/2}$ [7]. The values of all the constants used in this section are presented in Table 1.

The stream-wise component of the geostrophic wind U_g, i.e., the mean wind speed in the free atmosphere, is predicted using the geostrophic drag law:

$$\frac{\kappa U_g}{u_*} = \ln Ro_0 - A(Zi), \tag{2}$$

where $\kappa = 0.41$ is the von Kármán constant and $Ro_0 = u_*/(fz_0)$ is the surface Rossby number [16]. A is parameterized as

$$A = -A_1 m + \ln(A_0 + m) + \ln \beta, \tag{3}$$

where A_1 and A_0 are constant and m is the composite stratification parameter,

$$m = \left(1 + C_m^2 Zi^2\right)^{1/2} \beta^{-1}, \tag{4}$$

and

$$\beta = \left(C_R^{-2} + C_N^{-2} Zi\right)^{1/2}, \tag{5}$$

where C_R and C_N are constants.

The stream-wise wind component within the ABL consists of a logarithmic profile and an additional correction term:

$$\frac{\kappa U}{u_*} = \ln\left(\frac{z}{z_0}\right) + f_u(\xi, Zi), \tag{6}$$

where $\xi = z/h$ is the normalized height coordinate. The proposed expression for the correction is

$$f_u(\xi, Zi) = -a(Zi)\xi + a_\psi(Zi)\psi(\xi), \tag{7}$$

where

$$a_\psi = \frac{2-a}{1-2\epsilon}, \tag{8}$$

$$\psi = \xi - \frac{e^{\xi/\epsilon}-1}{e^{1/\epsilon}-1}, \tag{9}$$

and where ϵ relates the thickness of the entrainment layer to the boundary layer depth. Its value depends on Zi but it is possible to assume $\epsilon = 1.2$ for moderate Zi [9]. The value of $a(Zi)$ can be obtained from the continuity condition at the top of the ABL where $U(\xi = 1) = U_g$. Considering that $\psi(\xi = 1) = 0$ and combining Eq. (2) and (6) with $ln(Ro) = ln(b) + ln(h/z_0)$ at $\xi = 1$,

$$f_u(1, Zi) = \ln b - A \equiv -a(Zi). \tag{10}$$

2.2 Temperature profile

The potential temperature in a neutral boundary layer is constant across the ABL. However, in a CNBL the potential temperature increases in the entrainment layer with a slope that is proportional to inversion strength $\partial\theta/\partial z = \theta_0 N^2/g$. Any function matching this requirement could potentially be used. In this work we used the following formulation:

$$\theta(z) = \theta_0 \left[1 + \frac{N^2}{g} \ln(1 + e^{z-h(1-0.05^{2/3})})\right]. \tag{11}$$

The potential temperature can then be converted to temperature using the approximation found in [17],

$$\theta(z) = T(z) + \Gamma_{\text{dry}}(z - z_s), \tag{12}$$

where $\Gamma_{\text{dry}} = g/c_P = 9.8$ K/km is the dry air adiabatic lapse rate.

2.3 Simulations

The profiles from the previous sections were used to compute the corresponding sound fields at distances of up to 5 km using the implementation of the Crank-Nicholson parabolic equation from Wilson [18]. The constants and parameters used to compute the profiles are shown in Table 1. The source consisted of a monopole placed at $(x, y) = (0, 0)$. The simulations were performed only downwind, since this is the case where sound travels the furthest. The domain had a range of 5 km and a height ranging from 200 to 1000 m, depending on the ABL depth used in each case. A resolution of $\lambda/10$ was used in both directions. The ground was modelled as a grass field with flow resistivity σ, porosity φ and characteristic impedance calculated using Wilson's model [19] and whose values are shown in Table 1. The values of h ranged from 200 to 500 m in steps of 25 m. Also a height of 1000 m was considered as an extreme case. These values fit the distribution of the boundary layer depth found in [20]. We considered 20 values of N, equally spaced and ranging from 6 to 14 mHz, according to values found in [10]. Each combination of h and N was used to compute the correction term in Eq. (6). For each combination we computed a sound field produced by a profile using the correction term and one without, hence with a simple logarithmic profile. These pairs of sound fields were then compared to study the error introduced by using a logarithmic profile in a CNBL. We evaluated the differences between these sets of two sound fields using the MAC [21],

$$\text{MAC} = \frac{\left|\mathbf{p_{log}}^{\text{H}}\mathbf{p_{cnbl}}\right|^2}{\left(\mathbf{p_{log}}^{\text{H}}\mathbf{p_{log}}\right)\left(\mathbf{p_{cnbl}}^{\text{H}}\mathbf{p_{cnbl}}\right)}. \tag{13}$$

Further information on the nature of this error is obtained by studying the absolute phase and magnitude errors. The phase and magnitude errors were computed at each point in the domain and then averaged over the vertical coordinate up to 5 m above ground. The MAC was instead computed within regions of 50 m length and 5 m height, gradually sliding away from the source in steps of 25 m.

Table 1: Values and units of the constants and simulation parameters. The set of values for N and h are formatted as start value:step:stop value.

Parameter	Value	Unit
C_R	0.5	
C_N	1.6	
κ	1.4	
A_1	0.65	
A_0	1.3	
B_1	7	
B_0	8	
C_m	0.1	
ϵ	0.12	
f	0.0001	s^{-1}
θ_0	293	K
z_0	0.03	m
σ	200	kPasm^{-2}
φ	0.515	
N	6:0.42:14	mHz
h	200:25:500, 1000	m
$Z_{0,f=125Hz}$	12 + 11i	

3. RESULTS

This section presents the results obtained from the simulations. We show only the results at 125 Hz for space reasons and since they better show the effect of the ABL depth and inversion strength on the sound field. The same effects occur at larger distances as the frequency decreases. A subset of the profiles used to compute the sound fields are shown in Fig. 1, with and without the correction term, together with the corresponding effective speed of sound $c_{eff}(z) = c(T) + U(z)$. We then compared the sound fields resulting from these profiles with and without the correction term to asses the error introduced by using a logarithmic profiles in a CNBL.

Larger N produce larger wind speed, a steeper gradient close to the surface and a stronger inversion at the top of the boundary layer. This increases the height at which the gradient of the effective speed of sound changes sign and thus the extent of the down-refractive region of the medium. The height of the ABL has a similar effect, resulting in a larger wind speed and taller down-refracting region.

The MAC between the sound fields from these profiles and the corresponding logarithmic profile have been analyzed as a function of distance and ABL depth (Fig. 2), and inversion strength (Fig. 3). In general the two predictions diverge with distance, and the MAC drops dramatically between 1 km and 2 km. The deviation onset is closer to the source as N increases while a larger h produce more interference and larger larger spatial variations. Figure 2 shows the superposition of two patterns: one with low and another with high wavenumbers. The first occurs with any combination of N and h and is associated with the wind speed mismatch close to the ground. The ABL depth has a weaker influence on this pattern than N. However, the pattern starts slightly closer to the source as the height of the ABL increases. The high wavenumber pattern does not exist in shallow ABLs with a weak inversion. This pattern becomes more complex as the ABL depth increases. As the ABL gets taller, also the region where downward refraction occurs grows. Thus, the amount of energy refracted downwards also increases producing more complex interference at the ground.

The second pattern becomes more complex as the ABL depth and inversion strength increase. This can also be seen in Figure 3. This figure also shows two overlapping patterns as a results of different mechanisms affecting the MAC. The inversion strength N has a much larger influence on the low wavenumber pattern than h

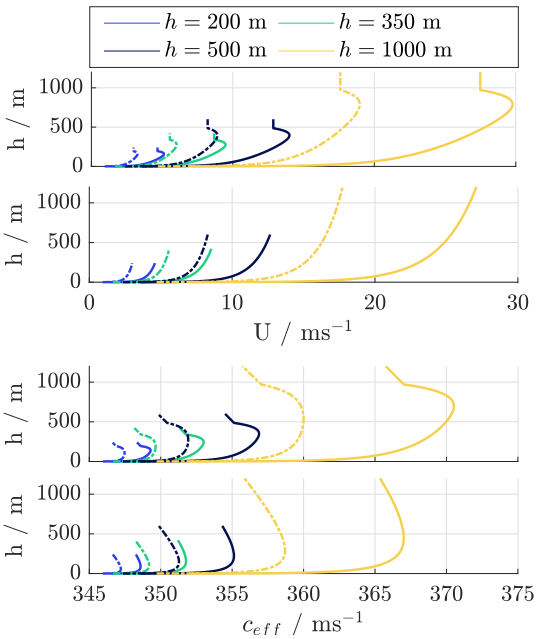

Figure 1: A subset of the profiles computed using Eq. (6). The first two plots from the top show the wind profiles with and without (logarithmic profile) the correction term, respectively. The last two plots show the corresponding profiles of the effective speed of sound. The profiles are shown for a subset of four different ABL depths (including the shallowest and the deepest) and two inversion strengths: the smallest ($N = 6$ mHz, dashed) and the largest ($N = 14$ mHz, solid).

does. The distance from the source where this pattern occurs is inversely proportional to N. The wavenumbers of this pattern are instead directly proportional to the inversion strength, i.e. as N increases the spatial variations of the pattern are larger. The inversion strength also affects the position where this second patter starts.

Figure 4 confirms that phase is the main culprit for the drop in MAC seen in the previous figures. Also here, we see the weak influence of h on the low wavenumber pattern and a larger influence on the high wavenumber one. Figure 5 shows instead how the inversion strength affects both patterns. Also this figure reflects quite well what presented in Figures 2 and 3.

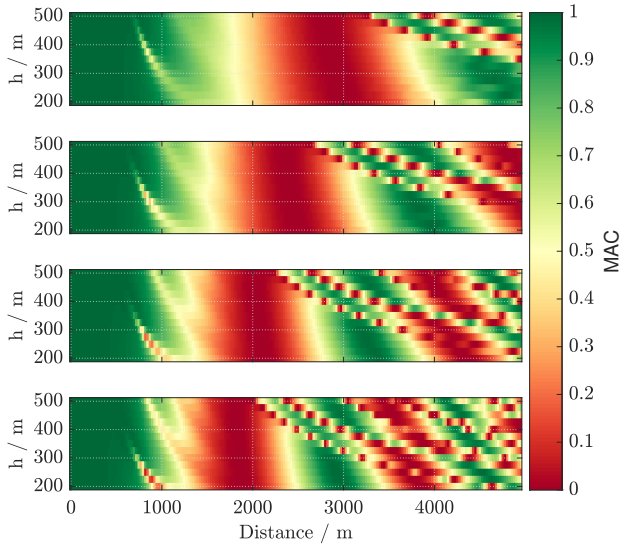

Figure 2: Four snapshots of the MAC at four different values of the inversion strength N (top to bottom): 6, 8.5, 11.5 and 14 mHz. Each plot shows the MAC as a function of distance from the source (horizontal axis) and ABL depth h up to 500 m (vertical axis).

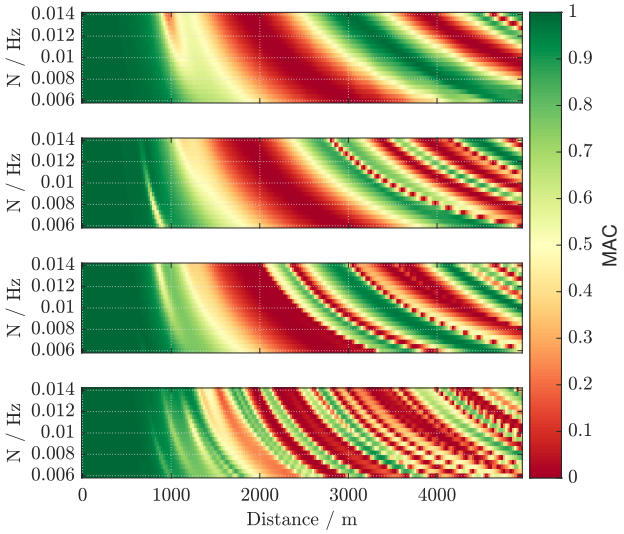

Figure 3: Four snapshots of the MAC at four different values of the ABL depth h (top to bottom): 200, 350, 500 and 1000 m. Each plot shows the MAC as a function of distance from the source (horizontal axis) and inversion strength N (vertical axis).

Figures 6 and 7 show the absolute magnitude error as a function of h and N. The magnitude error is small close to the source and resembles the pattern of the high wavenumber error found in MAC and phase. The magnitude error is relevant only where interference occurs. Before 2 km there is no interference and the magnitude of both sound fields is only affected by spherical divergence. Beyond 2 km, the direct, reflected and refracted waves interact. In this region, the discrepancy in wind speed and the amount of downward refracted energy generate different interference patterns, introducing a magnitude error. Notwithstanding the low magnitude error before 2 km, successful applications of sound field control would be limited to 1 km due to the phase error.

4. DISCUSSION

In the results we see how the magnitude error becomes relevant beyond 2 km, while the phase error can be as large as 60° at around 1 km. Beyond this distance the phase difference grows at a rate that largely depends on the inversion strength at the top of the ABL. In a sound field control application, a phase error of 60° marks the transition from noise reduction to amplification.

There are two main sources of error, visible as two different patterns. The low wavenumber pattern is the main source of error and is associated with the phase difference introduced by the wind speed mismatch close to the ground which is consistent with the findings in [15]. Without the ABL-capping inversion, the profile from Eq. 6 is equivalent to the logarithmic one. Subsequently, this pattern is only weakly affected by the ABL depth h while showing a strong dependence on inversion strength (N).

The high wavenumber pattern is instead coupled to both parameters. In general, a deeper ABL or a stronger inversion increases the height of the region where sound waves are refracted downward. As this region gets taller, the amount of downward refracted energy also increases and produces more complex interference at the ground. Since the correction term depends on both the inversion strength (stability condition given by N) and the normalized height coordinate ξ, they both affect the prediction error. Increasing N also moves this interference closer to the source. Compared to a logarithmic profile, the increase in N results in a steeper wind speed gradient around the ABL top. The steeper gradient reduces the radius of curvature of the sound rays, decreasing the dis-

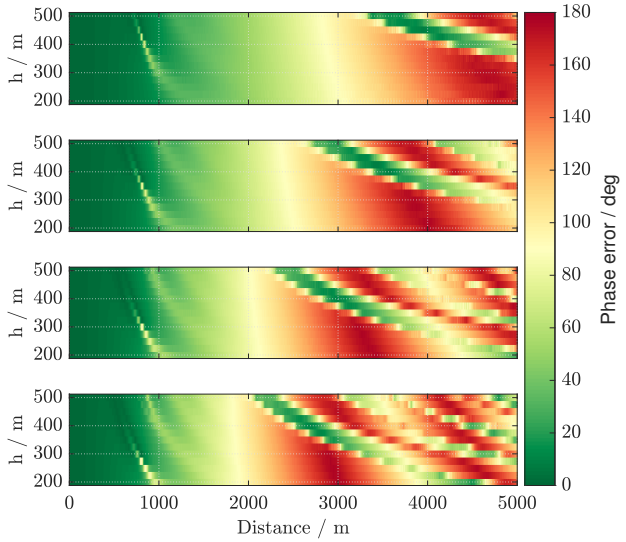

Figure 4: Four snapshots of the absolute phase error at four different values of the inversion strength N (top to bottom): 6, 8.5, 11.5 and 14 mHz. Each plot shows the absolute phase error as a function of distance from the source (horizontal axis) and ABL depth h up to 500 m (vertical axis).

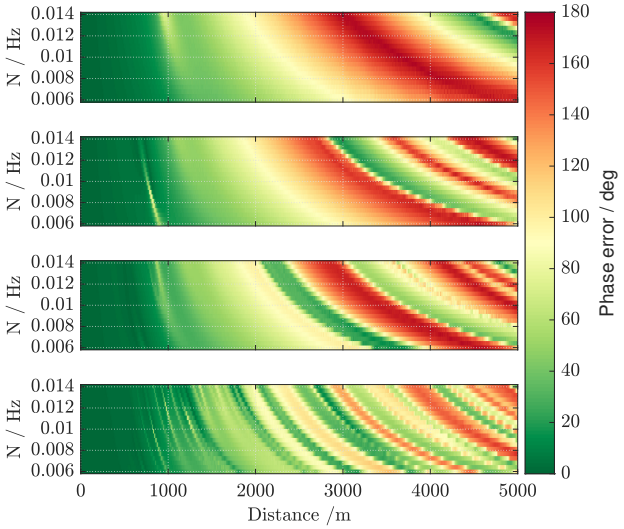

Figure 5: Four snapshots of the absolute phase error at four different values of the ABL depth h (top to bottom): 200, 350, 500 and 1000 m. Each plot shows the absolute phase error as a function of distance from the source (horizontal axis) and inversion strength N (vertical axis).

tance from the source where interference becomes significant. Furthermore, a stronger inversion produces a stronger upper-ABL jet; this increases the maximum elevation angle at the source that will result in downward refraction, when compared to a profile ignoring the ABL top.

The error introduced by using a logarithmic profile in a CNBL affects mainly the phase. The magnitude error becomes relevant beyond 2 km. From this distance, the refracted waves produce an error magnitude that is, however, confined to limited regions. On the other hand, the phase error can be as large as 45° already at 1 km and affect large portions of the domain.

The case considered here is representative for sound field control application for open air events [14,22], which often take place over grass and where sound sources are typically placed on the ground. In this study the position of the source and type of ground were chosen to limit the influence of ground reflections, to better isolate and study the influence of the propagation medium. Moving the source away from the ground produces reflections closer to the source that are not independent of the medium. A hard boundary allows such reflections to propagate over larger distances due to the reduced attenuation. In this scenario, the additional reflections produce more interference making it harder to analyze the effects produced by the medium alone and the different profiles. The resulting interference pattern is more complex and the interaction between direct and refracted wave would not be as clear.

5. CONCLUSION

In this work we analyzed the prediction error introduced by using a logarithmic profile in a CNBL, where it is not suitable due to the larger wind speed resulting from the stable stratification at the CNBL top. We described an alternative formulation for the wind and temperature profiles suited to a CNBL. This formulation is tested against a logarithmic profile by generating the two corresponding sound fields using the Crank-Nicholson parabolic equation. The two sound field are then compared through the MAC metric and in terms of the absolute phase and magnitude errors. For distances shorter than 1 km, both phase and magnitude errors are small and the two sound fields present a large spatial correlation. Beyond this distance, the prediction error appears as two overlapping patterns,

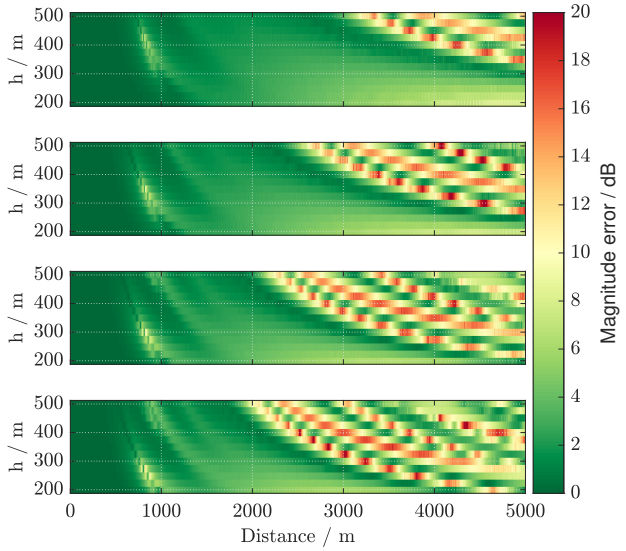

Figure 6: Four snapshots of the absolute magnitude error at four different values of the inversion strength N (top to bottom): 6, 8.5, 11.5 and 14 mHz. Each plot shows the MAC as a function of distance from the source (horizontal axis) and ABL depth h up to 500 m (vertical axis).

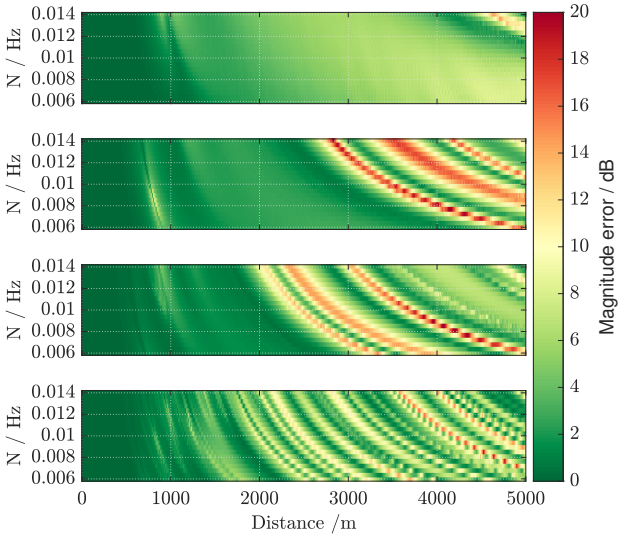

Figure 7: Four snapshots of the absolute magnitude error at four different values of the ABL depth h (top to bottom): 200, 350, 500 and 1000 m. Each plot shows the absoluite magnitude error as a function of distance from the source (horizontal axis) and inversion strength N (vertical axis).

one with low and one with high wavenumber. The former is the most important one since it affects large portions of the entire domain. It is mainly dependent on the inversion strength N and it is a results of the wind speed mismatch close to the ground. The ABL depth h has only a weak influence. The high wavenumber component instead depends on both parameters. When either of them increases, so does the error due to an increase in downward refracted energy. This increase results in more complex interactions between direct, refracted and reflected waves than with a logarithmic profile. The reason is an increase in the height of the downward refracting region due to an increase in h and an increase in the maximum turning angle due to H.

The magnitude error is relevant only in very limited regions far from the source (more than 2 km). The phase error instead is considerable at shorter distances (already at 1 km) and affects large regions of the domain. In cases where many sound sources are involved, it is crucial to limit such an error since the total sound field will not only inherit the phase error but the interaction between the sources will result in a larger magnitude error.

6. REFERENCES

[1] M. Kelly and S. E. Gryning, "Long-Term Mean Wind Profiles Based on Similarity Theory," *Boundary-Layer Meteorology*, vol. 136, no. 3, pp. 377–390, 2010.

[2] G. P. Van Den Berg, "Effects of the wind profile at night on wind turbine sound," *Journal of Sound and Vibration*, vol. 277, no. 4-5, pp. 955–970, 2004.

[3] S. Taherzadeh, K. M. Li, and K. Attenborough, "Some practical considerations for predicting outdoor sound propagation in the presence of wind and temperature gradients," *Applied Acoustics*, vol. 54, no. 1, pp. 27–44, 1998.

[4] M. Hornikx, R. Waxler, and J. Forssén, "The extended Fourier pseudospectral time-domain method for atmospheric sound propagation," *The Journal of the Acoustical Society of America*, vol. 128, no. 4, pp. 1632–1646, 2010.

[5] E. M. Salomons, "Caustic diffraction fields in a downward refracting atmosphere," *The Journal of*

the Acoustical Society of America, vol. 104, no. 6, pp. 3259–3272, 1998.

[6] F. Junker, B. Gauvreau, D. Ecotiére, C. Crémézi-Charlet, and P. Blanc-Benon, "Meteorological classification for environmental acoustics - practical implications due to experimental accuracy and uncertainty," in *19th International congeess on acoustics*, no. September, (Madrid), 2007.

[7] J. C. Wyngaard, *Turbulence in the Atmosphere*. Cambridge: Cambridge University Press, 2010.

[8] S. S. Zilitinkevich and I. N. Esau, "On integral measures of the neutral barotropic planetary boundary layer," *Boundary-Layer Meteorology*, vol. 104, no. 3, pp. 371–379, 2002.

[9] L. Liu, S. N. Gadde, and R. J. A. M. Stevens, "Geostrophic drag law for conventionally neutral atmospheric boundary layers revisited," *Quarterly Journal of the Royal Meteorological Society*, vol. 147, no. 735, pp. 847–857, 2021.

[10] M. Kelly, R. A. Cersosimo, and J. Berg, "A universal wind profile for the inversion-capped neutral atmospheric boundary layer," *Quarterly Journal of the Royal Meteorological Society*, vol. 145, no. 720, pp. 982–992, 2019.

[11] S. E. Gryning, E. Batchvarova, B. Brümmer, H. Jørgensen, and S. Larsen, "On the extension of the wind profile over homogeneous terrain beyond the surface boundary layer," *Boundary-Layer Meteorology*, vol. 124, no. 2, pp. 251–268, 2007.

[12] S. S. Zilitinkevich and I. N. Esau, "Resistance and heat-transfer laws for stable and neutral planetary boundary layers: Old theory advanced and re-evaluated," *Quarterly Journal of the Royal Meteorological Society*, vol. 131, no. 609, pp. 1863–1892, 2005.

[13] L. Liu and R. J. A. M. Stevens, "Vertical structure of conventionally neutral atmospheric boundary layers," *Proceedings of the National Academy of Sciences*, vol. 119, p. e2119369119, May 2022.

[14] P. Libianchi, F. T. Agerkvist, and E. Shabalina, "A review of techniques and challenges in outdoor sound field control," in *Proceedings of Inter·Noise 2022*, 2022. 51¡sup¿st¡/sup¿ International Congress and Exposition on Noise Control Engineering, Internoise 2022 ; Conference date: 21-08-2022 Through 24-08-2022.

[15] P. Libianchi, E. Shabalina, M. Kelly, J. Brunskog, and F. Agerkvist, "Sensitivity of the predicted acoustic pressure field to the wind and temperature profiles in a conventionally neutral boundary layer," 2023. Under review.

[16] M. van der Laan, M. Kelly, and M. Baungaard, "A pressure-driven atmospheric boundary layer model satisfying rossby and reynolds number similarity," *Wind Energy Science*, vol. 6, no. 3, pp. 777–790, 2021.

[17] R. B. Stull, *An Introduction to Boundary Layer Meteorology*. Dordrecht: Springer Netherlands, 1988.

[18] D. K. Wilson, "Outdoor sound propagation calculator," 2015. In: V. E. Ostashev and D. K. Wilson, Acoustics in Moving Inhomogeneous Media (second edition), Taylor & Francis.

[19] D. K. Wilson, "Relaxation-matched modeling of propagation through porous media, including fractal pore structure," *Journal of the Acoustical Society of America*, vol. 94, no. 2, pp. 1136–1145, 1993.

[20] S. Liu and X. Z. Liang, "Observed diurnal cycle climatology of planetary boundary layer height," *Journal of Climate*, vol. 23, no. 21, pp. 5790–5809, 2010.

[21] R. J. Allemang, "The modal assurance criterion - twenty years of use and abuse," *Sound and Vibration*, vol. 37, pp. 14–23, AUG 2003.

[22] P. Libianchi, J. Brunskog, F. Agerkvist, and E. Shabalina, "Active noise control at low frequencies for outdoor live music events using the conjugate gradient least square method," *Applied Acoustics*, vol. 205, 2023.